Masuda *Earth, Planets and Space* (2015) 67:204
DOI 10.1186/s40623-015-0377-x

Earth, Planets and Space
a SpringerOpen Journal

LETTER Open Access

Laboratory evidence of strength recovery of a healed fault: implications for a mechanism responsible for creating wide fault zones

Koji Masuda

Abstract

Fault zones consist of a high-strain fault core and a surrounding damage zone of highly fractured rock. The close, reciprocal relationship between fault zones and earthquake rupture evolution demands better understanding of the processes that create and modify damage zones. This study modeled the evolution of a damage zone in the laboratory by monitoring seismic signals (acoustic emissions) in a specimen of ultramylonite stressed to failure. The result provided evidence supporting the strength recovery of parts of the healed surface. A new fault initiated in an area of heterogeneous structure a short distance from the preexisting fault plane. Repeated cycles of fracture and healing may be one mechanism responsible for wide fault zones with multiple fault cores and damage zones.

Keywords: Fault zone, Acoustic emission, Healed fault, CT

Introduction

The structure and development of fault zones are closely related to the evolution of earthquake ruptures. Although fault zones occupy a small volume of the crust, they strongly affect crustal dynamic processes such as earthquakes and fluid flow in the crust (e.g., Faulkner et al. 2010). Fault zones consist of a core, in which strain is high and localized, surrounded by a highly fractured region called the damage zone (e.g., Chester and Logan 1986; Chester et al. 1993). Damage zones also influence fluid flow properties and the frictional strength of faults through their effects on pore pressure (Caine et al. 1996).

The dynamic processes responsible for creating off-fault damage have been modeled mostly on the basis of data obtained in field surveys of well-exposed damage zones (Blenkinsop 2008; Mitchell and Faulkner 2009; Fukuchi et al. 2014). Despite a wealth of field evidence and models, however, our understanding of these dynamic processes is incomplete. Recently, Valoroso et al. (2014) used high-resolution earthquake distributions to argue that during the coseismic phase of the seismic cycle, most of an earthquake's energy, which produces the damage zone, is concentrated along the main fault plane. At laboratory scale, Lockner et al. (1991) and Lockner (1993) investigated the evolution of acoustic emissions (AEs) in time and space and showed that AE clusters characterize the development of fault zones in intact rocks. Many earlier works have studied the effect of heterogeneity in a rock sample on failure processes (e.g., Lei et al. 2004; Jouniaux et al. 2001). These previous works show that precursory anomalies related to rock fracture are strongly dependent on the heterogeneity of the rock sample. In this study, I examined the strength recovery of a healed plane by comparing the locations of a preexisting healed plane and a new fracture plane. Fault zones are typically characterized by the presence of many healed surfaces, the strength of which is unknown. If a healed fault recovers its strength such that its strength is equal to or greater than that of the intact host rock, then repeated cycles of fracture and healing may be one mechanism producing wide fault zones with multiple fault cores and damage zones. In this paper, I present laboratory evidence supporting the strength recovery of at least some parts of a healed fault surface, obtained by using state-of-the-art AE monitoring and X-ray

Correspondence: koji.masuda@aist.go.jp
Geological Survey of Japan, National Institute of Advanced Industrial Science and Technology, AIST Central 7, 1-1-1 Higashi, Tsukuba 305-8567, Japan

computed tomography (CT) imaging techniques. Because of the well-established scale similarity of fault zones (Faulkner et al. 2010), loading experiments in the laboratory allow earthquakes and the evolution of fault zones to be studied under well-controlled conditions (e.g., Masuda et al. 2012).

Methods

The loading experiment was performed with a specimen of ultramylonite. The sample was selected because it had a healed previous fracture, and the purpose of the experiment was to examine strength recovery of the healed fault. The sample was collected from an exhumed fault zone along the Median Tectonic Line (MTL) in western Nagano Prefecture, central Japan (Kawachi et al. 1983). A specimen with medium grain size that had been affected by faulting activity was collected from an outcrop more than 50 m wide close to the MTL. The sense of shear was determined from the sample's microstructures; healed surfaces and foliation of the rock sample were interpreted to be parallel to the slip direction and slip surfaces. The presence of natural slip surfaces in the sample allowed the relationship between the existing internal structure and the creation and development of a new fault surface to be studied. The test specimen was trimmed to make a cylinder 50 mm in diameter and 100 mm long with its end faces parallel to within 0.01 mm (Fig. 1a). Although the plane of the healed fracture and the fracture plane were not exactly flat, they were parallel and partly overlapping. A vertical cross section through the cylinder perpendicular to the healed or main fracture plane was selected for this study (Fig. 1b, c). The inclination angle of the healed plane to the compression direction was about 20°, which is the most likely angle of shear fracture in granite at a confining pressure of 50 MPa (Paterson and Wong 2005, their figure 10). This angle is very close to the inclination angle of the created fracture. Six pairs of cross-strain gauges, each 6 mm long, were cemented to the sample surface to measure local strain in the central part of the sample. Volumetric strain was calculated as $\varepsilon_z + 2\varepsilon_\theta$, where ε_z is the axial strain and ε_θ is the circumferential strain. An array of 30 piezoelectric transducers with a resonant frequency of 2 MHz was also cemented to the surface, and then the whole assemblage was sealed in silicone rubber before the compression test.

A conventional triaxial compression test of the ultramylonite cylinder was conducted using a constant loading rate of 31.7 kPa s^{-1} under 50 MPa of confining pressure, which prevented initial cracks in the sample from having any effect. Macroscopic failure of the sample occurred when the applied differential stress reached 439 MPa, close to the strength under similar conditions of the intact granite host rock (e.g., Jouniaux et al. 2001). The transducers recorded AEs during the loading experiment. Velocities of P waves that propagated perpendicular to the loading axis were measured intermittently by the pulse transmission method and used to calculate the hypocenters of AE events. The space and time

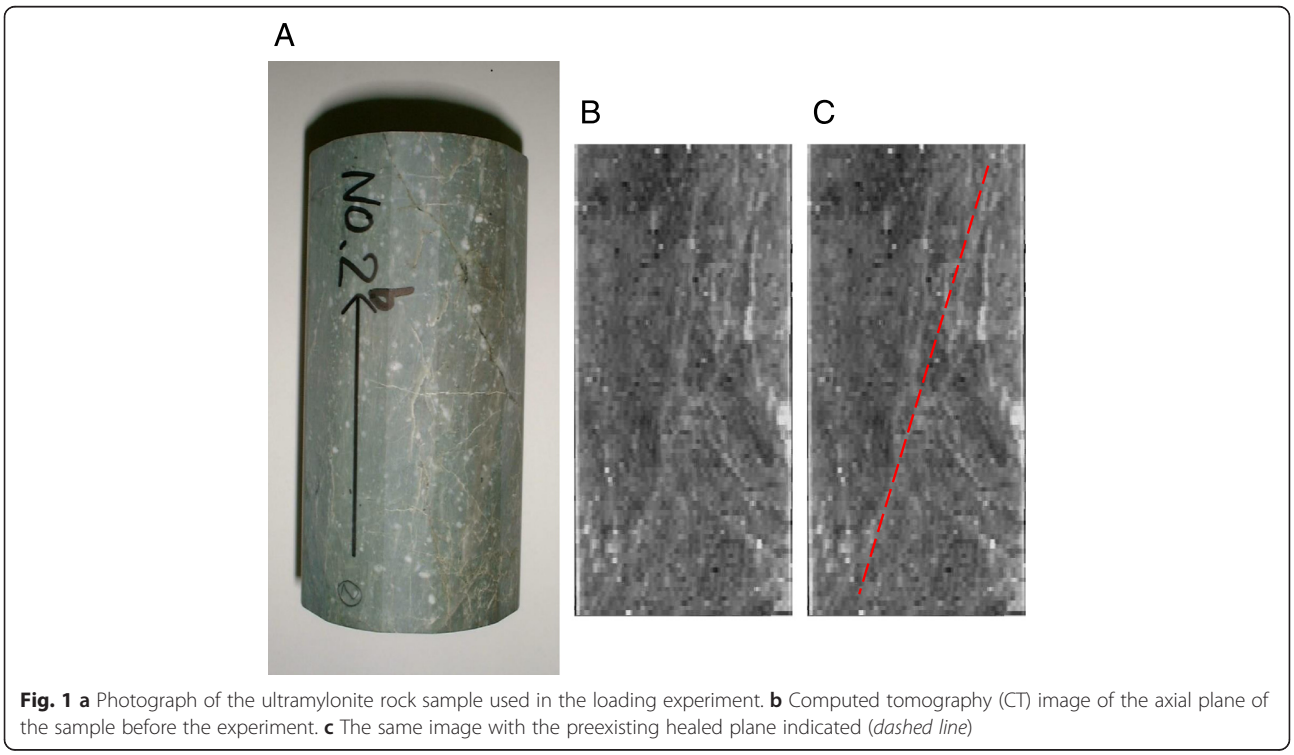

Fig. 1 **a** Photograph of the ultramylonite rock sample used in the loading experiment. **b** Computed tomography (CT) image of the axial plane of the sample before the experiment. **c** The same image with the preexisting healed plane indicated (*dashed line*)

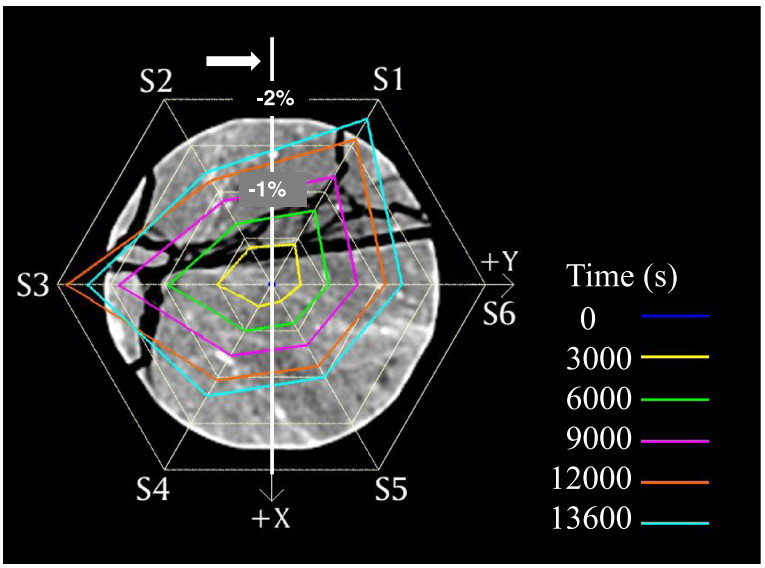

Fig. 2 Variations of local volumetric strain at six peripheral points on the sample surface at the midpoint of the specimen perpendicular to the loading direction. Expansion is considered positive. An X-ray CT image of a horizontal cross section through the sample obtained after the experiment is superimposed. The strike of the vertical cross section examined in this study is indicated by the *thick white line*, and the *thick white arrow* shows the direction from which the cross section is viewed in the other figures

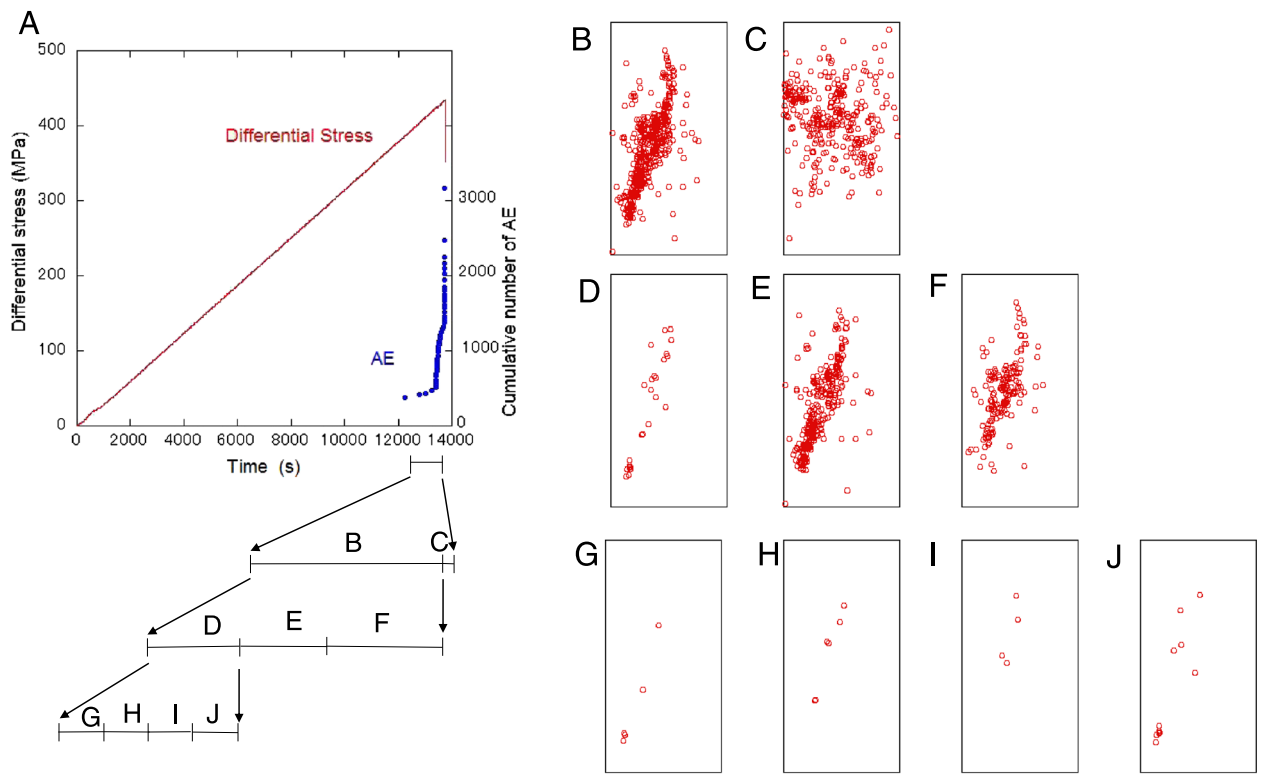

Fig. 3 Fault zone development as indicated by AE events. **a** Applied differential stress and the cumulative number of AE events plotted as a function of time. **b**–**j** The vertical cross section of the rock specimen showing AE event locations in nine time windows: **b** 12,500–13,720 s, **c** 13,720–13,740 s, **d** 12,500–13,000 s, **e** 13,000–13,500 s, **f** 13,500–13,720 s, **g** 12,600–12,700 s, **h** 12,700–12,800 s, **i** 12,800–12,900 s, and **j** 12,900–13,000 s

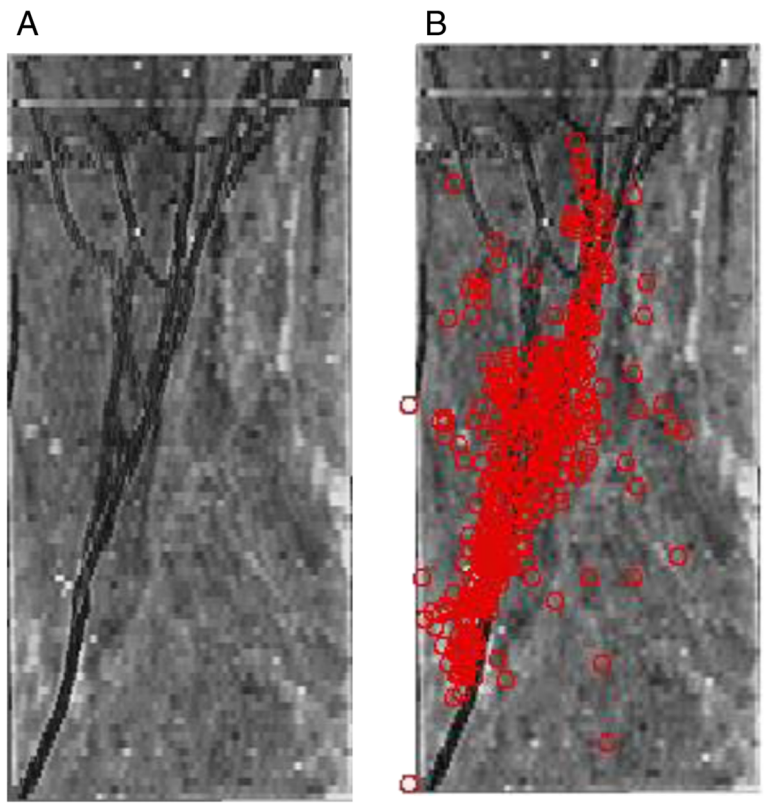

Fig. 4 CT images of the axial plane of the specimen. **a** After the loading experiment. Dark regions generally signify low bulk densities. **b** AE hypocenters between 12,500 and 13,500 s (Fig. 3b) plotted on the image shown in **a**

variations of AE source locations, which included the effects of heterogeneity and anisotropy of wave speed associated with accumulated damage in the rock sample during the deformation, were examined. Hypocenters were determined by automatically picking the first arrivals of P waves using the technique of Lei et al. (2004). Hypocenter locations with probability errors smaller than 2 mm (Lei et al. 2004) were used in this study.

The internal structure of the rock sample was imaged by X-ray CT before and after the loading experiment, using the method of Jouniaux et al. (2001). I used a conventional medical X-ray CT scanning system to obtain images of a scanned volume 160 mm in diameter in slices perpendicular to the sample axis; each slice was 1.0 mm thick and divided into a 512×512 voxel grid. The resolution of the resulting images was about 0.3 mm, and light-colored regions in the images corresponded to areas of high density. Density contrasts, which probably reflect the presence of pores and cracks in the internal structure, generally reflect the strength distribution in the sample rock. The slices were digitally combined into three-dimensional models displaying the shapes and locations of the preexisting and new fracture planes.

Results

Figure 2 shows the surface volumetric strains measured at the sample surface around the central part of the sample. An X-ray CT image of a horizontal cross section through the specimen at the strain gauge locations, obtained after the experiment, is superimposed. To show the deformation features, the volumetric strains are plotted at each of the indicated loading times. Strains measured until just before the rapid increase in AE activity are plotted. Therefore, this strain diagram shows the deformation from the start of the experiment to just before the volumetric increase due to dilatancy. During the loading, the volumetric strain at location S3, where the fracture plane eventually appeared at the sample surface, decreased more than the strain at the other locations. Although the AE activity increased just before the fracture, the strain was inhomogeneous in the early stage of loading. In symmetric compression tests of a homogeneous rock sample, microfractures in the sample are distributed homogeneously in sections perpendicular to the loading axis until the axial load reaches its peak value (e.g., Zang et al. 1998). In contrast, strain in this sample that included a healed plane became localized at the very early stage of loading. This result suggests that strength recovery is not uniform along

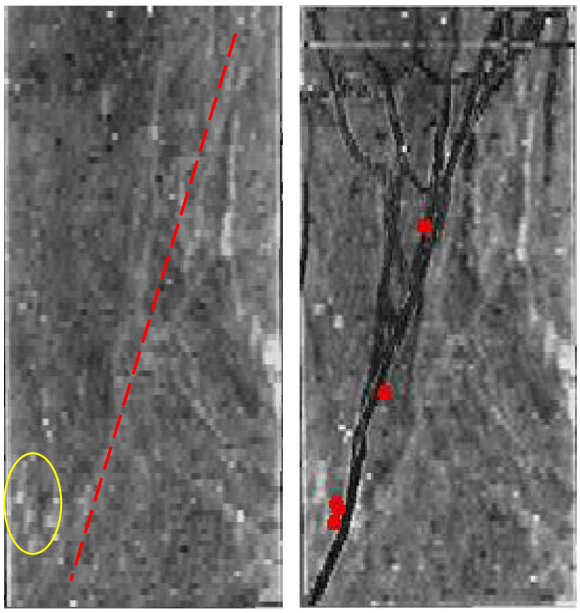

Fig. 5 CT images showing the relationship between spatial heterogeneity in the ultramylonite sample and AE events in the initial stage of fracture development, between 12,600 and 12,700 s (Fig. 3g). **a** Fracturing initiated a short distance from the preexisting damage plane in a heterogeneous region (within the *yellow oval*). The *dashed red line* indicates the preexisting healed plane. **b** Relationship of AE events during the earliest stage of fracture development (*red dots*) to later zones of failure (plotted on the same image as that in Fig. 4a)

the entire length of the fault, and at least some parts of the healed fault may be weaker than the host rock, leading to strain and AE localization during the early stage of loading.

AEs occurred late in the loading period (after 12,500 s) with the increase in the applied differential stress, and sample failure occurred abruptly at 13,740 s (Fig. 3a). The main fracture surface formed nearly parallel to the plane of the existing healed fracture. AE activity was concentrated around the fault plane (Fig. 3b) until 20 s before failure, when AEs became distributed throughout the sample (Fig. 3c). As the sample approached failure, acoustic activity occurred first along the future fault surface between 12,500 and 13,000 s (Fig. 3d), then in a wider region around the future fault zone (Fig. 3e), and finally in a zone extending farther along the future fault plane (Fig. 3f). Early in the initial period of AE activity (12,600–12,900 s), AEs began near the lower left corner of the vertical cross section selected for study (Fig. 3g). The upward propagation of AE activity was apparently accompanied by on and off AE activity in the lower left. The temporal variation in the AE source locations in the direction normal to the cross section was random, and they showed no systematic movement. The apparent upward propagation speed of AE activity along the fault plane on the cross section, estimated from the movement of the averaged positions for each time period corresponding to Fig. 3g-i was about 0.2 mm/s.

Discussion and conclusion

Before the loading experiment, CT images of the specimen showed a healed fault plane, identifiable by its light color as relatively dense material, crossing from the lower left to the upper right of the selected vertical cross section (Fig. 1b, c). The macrofracture surface created during the loading experiment (Fig. 4a) was very close to the preexisting healed plane, suggesting that the AE events reflected reactivation of the healed fault plane. The AE hypocenters during the time period leading up to failure (Fig. 3b) closely match the locations of both the preexisting healed surface and the new fault plane (Fig. 4b). Coseismic AEs, those occurring almost at the same time as the final fracture, were distributed throughout the specimen without favoring the fractured surface (Fig. 3c).

The structure of fault zones has been studied in field surveys of exhumed fault zones (Faulkner et al. 2003; Shigematsu et al. 2009). High-resolution earthquake locations determined in a field survey have shown a close relationship between seismicity and fault plane features (Valoroso et al. 2014), and high-resolution hypocenter determinations of natural seismicity have shown that active fault zones are narrow features (Hauksson 2010; Powers and Jordan 2010). Valoroso et al. (2014) speculated that coseismic deformation is concentrated along the main fault plane and is responsible for producing the observed damage zone structure. The loading experiment in this study corroborates these earlier observations.

The loading experiment also revealed details of the initial stage of fault development (Fig. 5). The new fault zone developed near, but not precisely on, the preexisting healed fault plane. The AEs began in an area of heterogeneous structure (Fig. 5a; light-colored patches within the yellow oval), where stress appears to have concentrated, and the fracture also started in that area (Fig. 5b). As mentioned in the "Methods" section, the inclination angle of the healed plane relative to the compression direction is most likely the angle of shear fracture in granite under a confining pressure of 50 MPa (e.g., Paterson and Wong 2005). However, in this experiment, the ultimate rupture did not occur on the healed plane. This result means that the healed surface was not a weak surface; rather, healing strengthened the fault so that its strength was equal to or greater than that of the intact host rock. The stress distribution near the edge of the specimen and in the lower part of the specimen, including the initial fracturing area and healed plane, was influenced by the lower end cap of the experimental apparatus. Under this circumstance, the

fracture initiated in an area of heterogeneous structure, as can be clearly seen on the CT image (Fig. 5a). Thus, the healing of the fault plane after the previous seismic event appears to have restored the rock to approximately its unfractured strength. These results suggest that repeated cycles of fracture and healing may be the main mechanism creating wide fault zones with multiple fault cores and damage zones.

Competing interests
The author declares that he has no competing interests.

Acknowledgements
Tomoaki Tomita contributed to the experimental part of this study and data analysis as a part of his master's thesis at the University of Tsukuba. Y. Kobayashi, O. Nishizawa, and X. Lei contributed to the early stages of this work. Constructive comments by the Editor and reviewers were very helpful to improve this manuscript. A part of this work was supported by JSPS KAKENHI Grant Number 15K06221.

Received: 12 August 2015 Accepted: 17 December 2015
Published online: 24 December 2015

References

Blenkinsop TG (2008) Relationships between faults, extension fractures and veins, and stress. J Struct Geol 30:622–632. doi:10.1016/j.jsg.2008.01.008
Caine JS, Evans JP, Forster CB (1996) Fault zone architecture and permeability structure. Geology 24:1025–1028. doi:10.1130/0091-7613(1996)024<1025:FZAAPS>2.3.CO;2
Chester FM, Logan JM (1986) Implications for mechanical-properties of brittle faults from observations of the Punchbowl fault zone, California. Pure Appl Geophys 124:79–106. doi:10.1007/BF00875720
Chester FM, Evans JP, Biegel RL (1993) Internal structure and weakening mechanisms of the San-Andreas fault. J Geophys Res 98:771–786. doi:10.1029/92JB01866
Faulkner DR, Lewis AC, Rutter EH (2003) On the internal structure and mechanics of large strike-slip fault zones: field observations of the Carboneras fault in southeastern Spain. Tectonophysics 367:235–251. doi:10.1016/S0040-1951(03)00134-3
Faulkner DR, Jackson CAL, Lunn RJ, Schlische RW, Shipton ZK, Wibberley CAJ, Withjack MO (2010) A review of recent developments concerning the structure, mechanics and fluid flow properties of fault zones. J Struct Geol 32:1557–1575. doi:10.1016/j.jsg.2010.06.009
Fukuchi R, Fujimoto K, Kameda J, Hamahashi M, Yamaguchi A, Kimura G, Hamada Y, Hashimoto Y, Kitamura Y, Saito S (2014) Changes in illite crystallinity within an ancient tectonic boundary thrust caused by thermal, mechanical, and hydrothermal effects: an example from the Nobeoka Thrust, southwest Japan. Earth Planets Space 66:1–12. doi:10.1186/1880-5981-66-116
Hauksson E (2010) Spatial separation of large earthquakes, aftershocks, and background seismicity: analysis of interseismic and coseismic seismicity patterns in southern California. Pure Appl Geophys 167:979–997. doi:10.1007/s00024-010-0083-3
Jouniaux L, Masuda K, Lei X, Nishizawa O, Kusunose K, Liu L, et al (2001) Comparison of the microfracture localization in granite between fracturation and slip of a preexisting macroscopic healed joint by acoustic emission measurements. J Geophys Res 106:8687–8698. doi:10.1029/2000JB900411
Kawachi Y, Yuasa M, Katada M (1983) Geology of the Ichinose District: Geological Survey of Japan, Quadrangle Series, scale 1:50,000, 1 sheet, 70p. text (in Japanese with English abstract, 6 p.).
Lei X, Masuda K, Nishizawa O, Jouniaux L, Liu L, Ma W, et al (2004) Detailed analysis of acoustic emission activity during catastrophic fracture of faults in rock. J Struct Geol 26:247–258. doi:10.1016/S0191-8141(03)00095-6
Lockner DA (1993) The role of acoustic emission in the study of rock fracture. Int J Rock Mech Min Sci Geomech Abstr 30:883–899. doi:10.1016/0148-9062(93)90041-B
Lockner DA, Byerlee JD, Kuksenko V, Ponomarev A, Sidorin A (1991) Quasi-static fault growth and shear fracture energy in granite. Nature 350:39–42. doi:10.1038/350039a0
Masuda K, Arai T, Fujimoto K, Takahashi M, Shigematsu N (2012) Effect of water on weakening preceding rupture of laboratory-scale faults: implications for long-term weakening of crustal faults. Geophys Res Lett 39:L01307. doi:10.1029/2011GL050493
Mitchell TM, Faulkner DR (2009) The nature and origin of off-fault damage surrounding strike-slip fault zones with a wide range of displacements: a field study from the Atacama fault system, northern Chile. J Struct Geol 31:802–816. doi:10.1016/j.jsg.2009.05.002
Paterson MS, T-f W (2005) Experimental rock deformation—the brittle field. Springer, New York
Powers PM, Jordan TH (2010) Distribution of seismicity across strike-slip faults in California. J Geophys Res 115:B05305. doi:10.1029/2008JB006234
Shigematsu N, Fujimoto K, Ohtani T, Shibazaki B, Tomita T, Tanaka H, et al (2009) Localisation of plastic flow in the mid-crust along a crustal-scale fault: insight from the Hatagawa Fault Zone, NE Japan. J Struct Geol 31:601–614. doi:10.1016/j.jsg.2009.04.004
Valoroso L, Chiaraluce L, Collettini C (2014) Earthquakes and fault zone structure. Geology 42:343–346. doi:10.1130/G35071.1
Zang A, Wagner FC, Stanchits S, Dresen G, Andresen R, Haidekker MA (1998) Source analysis of acoustic emissions in Aue granite cores under symmetric and asymmetric compressive loads. Geophys J Int 135:1113–1130. doi:10.1046/j.1365-246X.1998.00706.x